Transmission Response Measurements of Frequency-Translating Devices Using a Vector Network Analyzer

Christopher J. Clark, Andrew A. Moulthrop, Michael S. Muha, and Christopher P. Silva, *Member, IEEE*

***Abstract*—A new method for accurately determining the transmission response of frequency-translating devices (FTD's) is presented. The absolute amplitude and phase of the FTD under test is obtained using a vector network analyzer (VNA) and two test FTD's, where one FTD must have reciprocal frequency response characteristics. The characterization of single-sideband (SSB) FTD's is obtained in a straightforward manner by combining data from three VNA two-port swept measurements. The characterization of double-sideband (DSB) FTD's can be performed in the same manner as for SSB FTD's, or, more accurately, by combining data from six two-port swept baseband measurements. A complete analysis of the characterization method using low-pass equivalent (LPE) signals and systems is presented, along with the development of the appropriate data reduction procedures needed to arrive at the de-embedded LPE FTD transmission responses. The validation and accuracy of the method is demonstrated with results for both SSB and DSB FTD's operating at 20 GHz.**

I. Introduction

THE MEASUREMENT of the transmission response of devices in a communications channel is essential for accurate systems modeling. Both the amplitude and phase response are needed to assess the extent of signal distortion. The most common tool for characterizing nonfrequency-translating components is the vector network analyzer (VNA). Due to their design and error correction capabilities, they are very fast and accurate. Frequency-translating devices (FTD's), such as mixers, are more difficult to characterize due to the frequency offset between input and output, and hence cannot be measured by a VNA alone. The technique described in this paper uses test FTD's (which we will take to be mixers for the rest of this paper) so that the frequency at the reference and test channels is the same. In this way, VNA's can be used to characterize FTD's with accuracies near those obtained for non-FTD's.

The most common FTD measurement technique uses a network analyzer and a reference test mixer to obtain the amplitude and phase match between FTD's [1]. This technique is limited in that it only provides the absolute difference between FTD's over a specified frequency range. In an extension of this technique, the transmission response of an FTD can be estimated relative to a "gold standard." The disadvantage of this approach is that the accuracy will always be limited to how well the standard has been characterized. Scalar network analyzers can be configured to accurately obtain the conversion loss of FTD's [2]. However, this technique does not completely characterize an FTD since phase information is not included. A technique has recently been developed that uses a microwave transition analyzer (MTA) [3]. The MTA technique uses AM or FM envelope delay to characterize SSB FTD's to 40 GHz, without the need for reference or test mixers. As a result, this technique has the additional capability of characterizing FTD's with inaccessible internal local oscillators (LO's). Compared to the new technique described in this paper, the limitations of the MTA technique are that it cannot characterize DSB FTD's and exhibits lower measurement speed and accuracy for SSB FTD's [4].

This paper presents a new method for accurately obtaining the transmission response of FTD's, which can range from a simple mixer to a complete communications channel with offset frequencies. The technique uses the VNA and provides an inferred response based on several measurements involving the swapping of test mixers. Only two test mixers are required in addition to the device-under-test (DUT), and one FTD must provide reciprocal frequency response characteristics. In a typical communications channel, FTD's are often operated as single-sideband (SSB) mixers in frequency converters. However, FTD's are also often used as double-sideband (DSB) mixers in modulators and demodulators. For example, in a biphase-shift-keying modulator, a DSB mixer is often used to upconvert a baseband digital signal. The method described in this paper applies to both SSB and DSB FTD's. This is the only method known by the authors for characterizing both the amplitude and phase response of a DSB FTD. It will be shown that the measurement of SSB FTD's can be performed quickly and accurately with only three VNA measurements. The measurement of DSB FTD's can be accomplished in two ways, defined by the choice of frequency range for the VNA swept measurement. The paper covers the test system configuration, signal analysis, and measurement results for this new approach. The validation and accuracy of the approach is demonstrated with results for both SSB and DSB FTD's operating at 20 GHz.

II. Test System Configuration

The test setup for the measurement of FTD's is shown in Fig. 1. For our work, we used a standard HP 8510C VNA which is capable of measurements from 0.05 to 50 GHz.

Manuscript received April 2, 1996.

The authors are with The Aerospace Corporation, Los Angeles, CA 90009 USA.

Publisher Item Identifier S 0018-9480(96)08546-8.

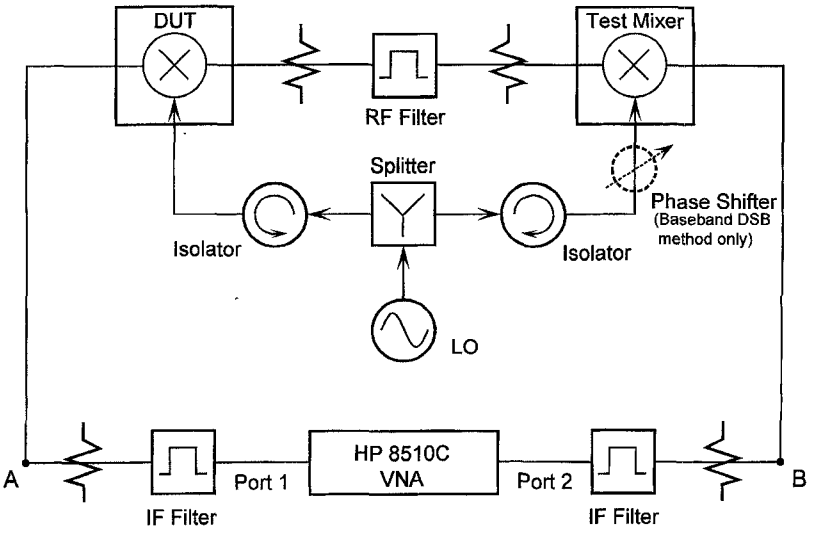

Fig. 1. General FTD test configuration.

In addition to the DUT and the VNA, a minimum of two test mixers, three filters, and four attenuators are used. It is recommended that the VNA perform its measurements at the lower of the two input/output FTD frequencies [e.g., the intermediate frequency (IF) of a mixer]. The configuration shown in Fig. 1 is therefore an example of a measurement of an upconverting DUT. The phase shifter on one LO arm is only required for one of the two DSB converter characterization methods. The test mixers are required to translate the first device's output back to the original input frequency. The filters and attenuators are used to minimize measurement error. The reference plane for the two-port measurement is located at points A and B. A full two-port calibration allows for very accurate results because the VNA measurements automatically incorporate full 12-term error correction. It should be emphasized that only a transfer function for each FTD is derived by this method; the VSWR effects between the two FTD's are not removed. Thus, these results should only be applied when the DUT is embedded in a well-matched system. Note that the technique requires that the DUT either has an external LO input or provides its internal LO as an output. This is necessary for the VNA to perform a phase coherent measurement. All the data collection and analysis presented here have been fully automated using software routines written in the LabVIEW®. application [5]. This greatly simplifies the measurement procedure and reduces the possibility of operator error.

A. SSB FTD Measurement Description

The transmission response of an SSB DUT can be inferred from the overall response of the DUT with a combination of test mixers. A minimum of two test mixers must be used, and additional test mixers can be used to improve accuracy. For SSB characterization, the IF filters shown in Fig. 1 are bandpass. A full two-port VNA measurement provides two transmission responses (s_{21} and s_{12}) for each mixer combination test case. When two test mixers are used, three test cases provide the following six results:

M_A: DUT + Test Mixer 1 (s_{21})
$M_{A'}$: Test Mixer 1 + DUT (s_{12})
M_B: DUT + Test Mixer 2 (s_{21})
$M_{B'}$: Test Mixer 2 + DUT (s_{12})
M_C: Test Mixer 1 + Test Mixer 2 (s_{21})
$M_{C'}$: Test Mixer 2 + Test Mixer 1 (s_{12})

where $M_X = M_X(\omega)$ represents the measured transfer function. Assuming DUT and test mixer reciprocity, our analysis will show that eight low-pass equivalent (LPE) responses can be calculated for the DUT (to within a fixed phase offset)

$$\{R_{\mathrm{DUT}}\}_{n=1}^{8} = \frac{\{R_A, R_{A'}\} + \{R_B, R_{B'}\} - \{R_C, R_{C'}\}}{2} \tag{1}$$

where $R = R(\omega)$ represents the amplitude (dB) or phase (degrees) portion of the corresponding total baseband equivalent measured response $M(\omega + \omega_u)$, where ω_u is the center frequency of the sweep; R_{DUT} is the calculated LPE response of the DUT; and $\{R_X, R_{X'}\}$ means choose one of the derived responses $R_X(\omega)$ or $R_{X'}(\omega), X = A, B, C$. Equation (1) applies to upper-sideband (USB) FTD's where the upconversion uses high-side injection and the downconversion uses low-side injection. For lower-sideband (LSB) FTD's, the upconversion and downconversion use high-side injection, and thus $R_{\mathrm{DUT}}(\omega)$ must be replaced by $R_{\mathrm{DUT}}(-\omega)$ if it is an amplitude and $-R_{\mathrm{DUT}}(-\omega)$ if it is a phase.

The application of this technique requires that at least one of the FTD's have reciprocal frequency response characteristics. This means that one of the FTD's must provide an identical transmission response whether used as an upconverter or downconverter. The best way to verify FTD reciprocity is by checking for the equality of s_{21} and s_{12} when combining two reciprocal FTD's back-to-back. The topology and application of a given FTD will determine whether it possesses this property. We have found that commonly used double- and

triple-balanced mixers exhibit this property when operated linearly and their ports are properly terminated. Since these mixers also provide high dynamic range and multi-octave bandwidth, they are ideally suited as test mixers for this technique. Note that for each nonreciprocal FTD used, there is a subsequent reduction in the number of valid responses that can be calculated from (1). For example, if test mixer 1 is the only reciprocal device, the only valid DUT response is calculated by using $R_X, X = A, B, C$ *or* $R'_X, X = A, B, C$. The first set characterizes the DUT as an upconverter, while the second set characterizes the DUT as a downconverter. When there is more than one reciprocal device, the accuracy of the derived DUT response can be increased by averaging the multiple valid responses that result.

B. DSB FTD Measurement Description

In this case, there are two VNA measurement methods, delineated by the choice of FTD frequency range (RF or baseband) for the VNA sweep. In the first method (the RF DSB method), the RF frequency range is chosen and the same SSB technique described above can be directly applied. The same measurement setup shown in Fig. 1 holds here as well, except that RF bandpass filters would be placed at the VNA ports instead, and a low-pass filter would be used between the two DSB FTD IF ports.

In most instances, more accurate results can be obtained by the baseband DSB method, which uses the baseband FTD frequency range for the VNA sweep, and requires a minor modification of the SSB measurement technique. First, using the same setup shown in Fig. 1, the VNA signal is applied to the IF ports of the FTD's and the IF filters at the VNA ports are low-pass. Second, the back-to-back FTD responses must be measured at *two* settings of the phase shifter that are 90° apart at the LO frequency, in order to completely characterize the FTD's.

The concept behind the baseband DSB method can be explained as follows. The baseband VNA output signal mixes with the LO in the DUT to produce both USB and LSB signals. Both sidebands are downconverted in the test mixer back to the baseband IF frequency. The sidebands recombine at any relative phase, based on the setting of the phase shifter. For example, if one setting of the phase shifter gives a maximum IF signal at a given IF frequency, then a setting 90° away will give a minimum IF signal. At the maximum IF signal, the two sidebands are in-phase, so the IF response is the sum of the two sideband responses. At the minimum IF signal, the sidebands are out-of-phase, so the IF response equals the difference of the two sideband responses. This is only an example; in practice it is unnecessary to find the maximum IF response—any two phase settings 90° apart are sufficient.

Our analysis will show that LPE DSB transmission response of the back-to-back FTD pairs is given by (to within a fixed phase offset)

$$\Pi(\omega) = \begin{cases} \frac{1}{2}[M_{\mathrm{I}}^*(-\omega) + \jmath M_{\mathrm{II}}^*(-\omega)], & \omega \le 0 \text{ (LSB response)} \\ \frac{1}{2}[M_{\mathrm{I}}(\omega) + \jmath M_{\mathrm{II}}(\omega)], & \omega \ge 0 \text{ (USB response)} \end{cases} \quad (2)$$

where the superscript "*" denotes the complex conjugate operation, $\jmath$ is the square root of -1, $M_{\mathrm{I}}(\omega)$ is the complex s_{21} response of the back-to-back FTD pairs at phase shifter setting I, and $M_{\mathrm{II}}(\omega)$ is the complex s_{21} response of the back-to-back FTD pairs at phase shifter setting II (setting II − setting I = +90°). Once the USB and LSB response of the DSB FTD are separated using (2), above, the DUT response can be derived by applying (1) (M replaced by Π) to each sideband independently. Thus for the baseband DSB method, the measurement process is similar to that performed for SSB FTD's except that for each of the three test cases, an additional measurement and calculation is made. The choice between the two DSB measurement methods should be based on achieving the best measurement accuracy and is determined by the characteristics of the specific FDT's under test.

C. FTD Measurement Precautions

Taking certain precautions in an FTD test setup can minimize the extent of measurement errors. The first consideration is the port termination sensitivities of the FTD's in the test configuration. Stand-alone mixers will often require special care in contrast to frequency converter units where isolation is often provided by filters, isolators, or amplifiers. As indicated earlier, our measurement technique does not account for errors due to VSWR interaction between the FTD's. Consequently, the VSWR of the test mixers should be low. In addition, it is known that many broadband mixers are especially sensitive to reactive port terminations [6]. The IF port is particularly sensitive since unwanted mixing products can be reflected back into the mixer generating erroneous secondary IF signals. Broadband resistive attenuators placed between the FTD's will serve to minimize VSWR interaction, as well as terminate spurious mixing products. The attenuation value required is based on the specific characteristics of the FTD's and termination, and is typically 6 to 10 dB. In cases where excessive loss cannot be tolerated, broadband isolators, diplexers, or constant impedance filters may be used.

The second measurement consideration is filtering. The RF filter used between the DUT and the test mixer in Fig. 1 is required to remove unwanted mixing products. These spurious signals generated by the DUT would otherwise interact in the test mixer resulting in measurement error. The filter bandwidth should be wider than the desired response bandwidth yet narrow enough to adequately reject the largest spurious signals. The response of the filter between the FTD's and accompanying attenuators are included in the measurement and can be removed mathematically. The filters on the VNA ports prevent spurious products generated by the mixers from causing measurement error within the VNA. The response of these filters and accompanying attenuators is removed by the calibration process.

III. FTD Modeling and Signal Analysis

This section will present the analytical foundations for our technique, beginning with the system modeling of the two basic FTD classes, followed by a derivation of the frequency response for cascaded nonfrequency-translating FTD pairs. An

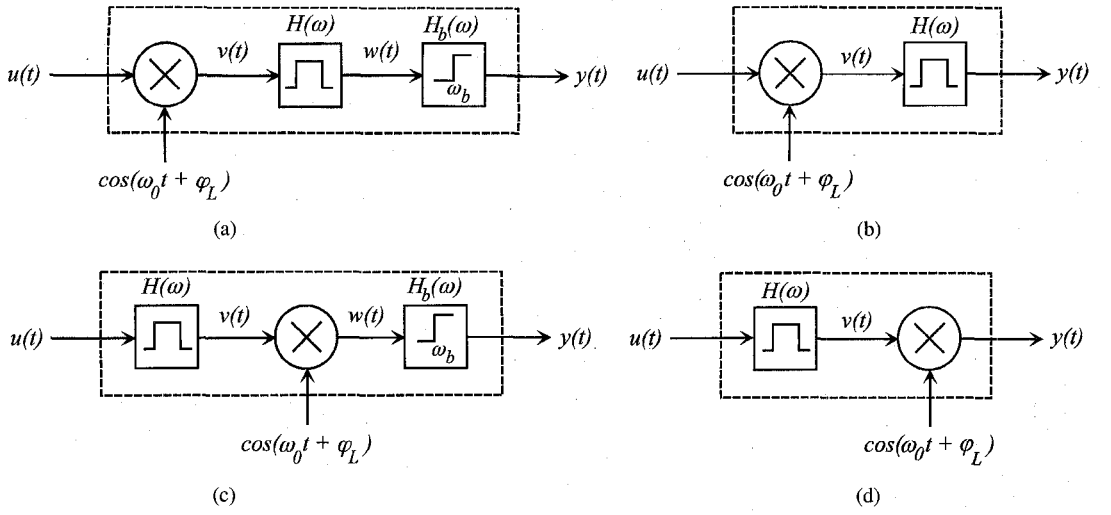

Fig. 2. Translator-filter (TF) and filter-translator (FT) forms of the basic FTD model structures. (a) TF SSB model (USB case: the LSB case is entirely similar). (b) TF DSB model. (c) FT SSB model (USB case: the LSB case is entirely similar). (d) FT DSB model.

LPE transmission response is then defined for each FTD class, which can be derived from input/output measurements on cascaded FTD pairs. It will be shown that such a response for a given DUT can be calculated from a set of basic linear algebraic equations.

A. Basic FTD Model

The basic FTD model that forms the basis for our analysis comes in two classes: 1) the SSB model that represents the simpler and more common mode of operation for FTD's and 2) the DSB model whose components can be ascertained in either of two ways. Furthermore, each class comes in two forms: 1) the translator-filter (TF) form wherein a perfect frequency translator is followed by a bandpass filter (which represents the FTD transmission response characteristics) and additionally an ideal brickwall filter for the SSB class and 2) a complementary filter-translator (FT) form in which the bandpass filter is followed by an ideal translator which in turn is followed by the brickwall filter for the SSB class. The TF models are used for FTD's that perform low-pass-to-bandpass (LP–BP) or bandpass-to-bandpass (BP–BP) translation, whereas the FT models represent FTD's with bandpass-to-low-pass (BP–LP) or BP–BP translations. In practice, SSB FTD's perform BP–BP translations, whereas DSB FTD's perform LP–BP and BP–LP conversions. We emphasize that the basic filter in the two models representing the imperfect translation of the FTD is always bandpass, and that both models can be used for BP–BP translations, the one chosen usually dictated by symmetry considerations. Fig. 2 illustrates the TF and FT forms for each model class, and the more common USB instance for the SSB model, as indicated by the high-pass brickwall filter H_b. The LSB case of the SSB model would contain a low-pass brickwall filter instead. Note from Fig. 2 that the FT model is a symmetrical reflection of the TF model for the DSB class, in contrast to the SSB class where the order of the elements has been rearranged.

We now describe in detail the general FTD model by listing the elements of each model class, including all assumptions made.

1) SSB FTD Model:

1) $u(t)$—Bandlimited input signal that is either baseband with bandwidth B_u (TF model form only) or bandpass, centered at ω_u satisfying $B_u \leq \omega_u$ (both model forms).
2) Ideal Multiplier—For the TF model form, provides frequency translation to: (a) the frequency ω_0 for baseband $u(t)$ where additionally $\omega_0 \geq B_u$ for the LSB case; and (b) the frequency $\omega_0 \pm \omega_u$ for bandpass $u(t)$ where $+$ $(-)$ corresponds to the USB (LSB). For the FT model form, only case (b) arises for $v(t)$ instead, with ω_u replaced by ω_v (which could equal ω_0). For both model forms, the constant φ_L represents the arbitrary phase of the LO relative to time $t = 0$, and is included to allow the general case in which the upconversion and the downconversion are accomplished with separate LO's.
3) $v(t)$—Translated bandpass output of the ideal multiplier for the TF model form or the bandpass filter H for the FT model form.
4) $H(\omega)$—Bandpass filter centered at ω_h with single-sided bandwidth B_h that filters $V(\omega)$ for the TF model form, $U(\omega)$ for the FT model form, and represents the essential frequency response characteristic of the FTD.
5) $w(t)$—Filtered bandpass output of $H(\omega)$ for the TF model form or output of the ideal multiplier for the FT model form.
6) $H_b(\omega)$—Brickwall filter centered at ω_b used to remove one of the sidebands of the DSB output from $H(\omega)$ (TF model form) or $W(\omega)$ (FT model form). Explicitly

$$H_b(\omega) = \begin{cases} 1, & |\omega| \geq \omega_b \\ 0, & |\omega| < \omega_b \end{cases} \quad \text{(USB Case)} \tag{3a}$$

$$H_b(\omega) = \begin{cases} 1, & |\omega| \leq \omega_b \\ 0, & |\omega| > \omega_b \end{cases} \quad \text{(LSB Case)} \tag{3b}$$

Note that H_b is an ideal high-pass (low-pass) filter for the USB (LSB) case.

7) $y(t)$—Output of the FTD that may be either baseband (FT model form only) or bandpass (both model forms) with corresponding bandwidth $B_y = B_h \leq B_u$.

2) DSB FTD Model: For this class, the model would simply consist of elements (1)–(4), and (7) from the SSB FTD model.

These models will be cascaded to form a nonfrequency-translating FTD pair and analyzed in the following subsection, beginning with the more general DSB class, followed by the simpler special SSB class case.

B. Cascaded FTD Model and Analysis

Fig. 3 provides a block diagram of the proposed cascaded FTD models that apply to both the SSB and DSB classes, with both FTD's being of the same class. Fig. 3(a) shows the model to be used for all SSB FTD's and the baseband DSB method, wherein, without loss of generality, FTD 1 is a TF-type upconverter, while FTD 2 is an FT-type downconverter. Note that for SSB FTD's, FTD 1 can be either USB or LSB, whereas FTD 2 must be LSB in order to arrive at a nonfrequency-translating cascade. This model represents the most accurate measurement configuration since the VNA sweeps the lower frequency range of the given FTD's.

Fig. 3(b) represents the model for the RF DSB method, where the translator forms and conversion directions of FTD 1 and FTD 2 are reversed in order to gain procedural simplicity with some possible sacrifice in measurement accuracy. In both models, the harmonic filter $H_o(\omega)$ will be ideal, bandpass or baseband as appropriate, and such that the frequency content of the output $z(t)$ is an untranslated and filtered form of that for $u(t)$. Also for the sake of generality, two separate LO's are shown, coherently locked to the same frequency ω_0, but with possibly differing phases φ_{L1} and φ_{L2} caused by path discrepancies between the master oscillator and the two FTD LO inputs. Finally, when the model is to be used to represent the operation of the FTD cascade in the reverse direction, the harmonic filter in Fig. 3(a) would be placed after the former input of FTD 1 instead, while all FTD's would be modeled by the complementary translator form for both FTD cascades.

1) Low-Pass Equivalent Signals and Systems: The analysis to be presented next for each of the FTD classes will be based on the concept of LPE signals and systems [7]–[9] that is reminiscent of the complex phasors used for sinusoidal steady-state analysis. Before proceeding with the FTD model analysis, we first will briefly review the relevant features of LPE theory.

For a general real signal $x(t)$ with a Fourier transform $X(\omega)$, we define the *analytic signal* or *preenvelope* of $x(t)$ by the complex signal

$$z_x(t) := x(t) + \jmath\hat{x}(t) \tag{4a}$$

where

$$\hat{x}(t) = \mathcal{H}[x(t)] := x(t) \circledast \frac{1}{\pi t} = \frac{1}{\pi}\int_{-\infty}^{\infty} \frac{x(\tau)}{t-\tau}\, d\tau \tag{4b}$$

is called the *Hilbert transform* of $x(t)$, and $\circledast$ denotes the convolution operator. Interpreted as a filter, the Hilbert transform is known as a *quadrature filter* since it introduces a phase shift of $\pm(\pi/2)$ in $X(\omega)$. It can be shown that in the frequency domain

$$Z_x(\omega) = 2X(\omega)U(\omega), \quad \hat{X}(\omega) = -\jmath X(\omega)\,\mathrm{sgn}(\omega) \tag{5}$$

where

$$U(\omega) := \begin{cases} 1, & \omega \geq 0 \\ 0, & \omega < 0 \end{cases}, \quad \mathrm{sgn}(\omega) := \begin{cases} 1, & \omega \geq 0 \\ -1, & \omega < 0 \end{cases} \tag{6}$$

are the *unit step* and *signum* functions, respectively.

Now suppose $x(t)$ is a bandpass signal with double-sided bandwidth $2B_x$ and centered at $\omega_x \geq B_x$ for positive ω. Let ω_0 be a reference frequency such that $\omega_x - B_x < \omega_0 < \omega_x + B_x$, that is, it falls within the bandwidth of $X(\omega)$ and satisfies

$$\omega_0 \geq \frac{\omega_x + B_x}{2}. \tag{7}$$

The reference frequency ω_0 is usually chosen to be the center frequency ω_x for simplicity and since condition (7) will be automatically satisfied. However, our analysis will need to allow for the more general choice of ω_0 for the FTD bandpass filters, since their center frequency ω_h need not equal the LO frequency ω_0 that we will choose as the reference frequency [see right-hand side of Fig. 4(a)]. Under these assumptions, it follows that $z_x(t)$ in (4) can also be written as

$$z_x(t) =: \tilde{x}(t)e^{\jmath\omega_0 t} \tag{8a}$$

where

$$\tilde{x}(t) := z_x(t)e^{-\jmath\omega_0 t} \tag{8b}$$

is termed the *LPE signal* or the *complex envelope* of $x(t)$ with respect to the reference frequency ω_0. In view of (5) and (8b), the Fourier transform $\tilde{X}(\omega)$ of $\tilde{x}(t)$ is given by

$$\tilde{X}(\omega) = Z_x(\omega + \omega_0) = 2X(\omega + \omega_0)U(\omega + \omega_0). \tag{8c}$$

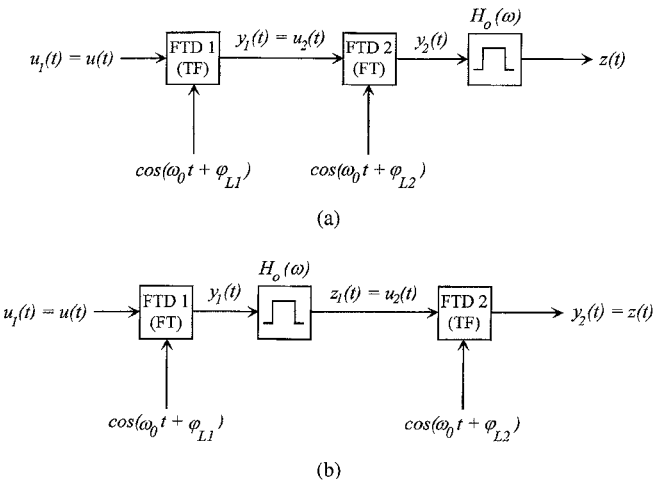

Fig. 3. Cascaded FTD models. The details of the individual FTD boxes have been provided in Fig. 2. The output filter $H_o(\omega)$ is used to remove unwanted harmonics in the signals produced by the two FT-type FTD's. (a) Model for SSB FTD's and DSB FTD's, the latter measured at baseband. (b) Model for DSB FTD's measured at RF.

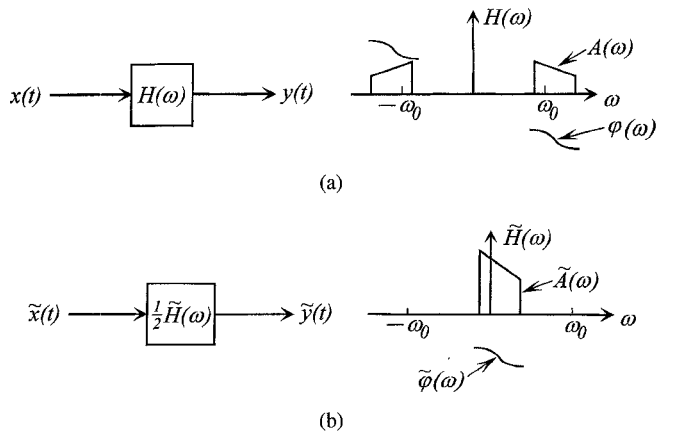

Fig. 4. Bandpass to low-pass equivalent filter transformation with respect to a reference frequency ω_0. (a) General bandpass filter $H(\omega)$ with amplitude component $A(\omega)$ and phase component $\varphi(\omega)$ (asymmetric and not frequency centered about ω_0). (b) Low-pass equivalent filter $\tilde{H}(\omega)$ with corresponding components $\tilde{A}(\omega)$ and $\tilde{\varphi}(\omega)$, and where $\tilde{x}(t)$ and $\tilde{y}(t)$ are the complex envelopes of the input $x(t)$ and output $y(t)$, respectively.

We can now define an LPE system as follows (see Fig. 4). Suppose $x(t)$ is as just described, and we have a linear system with real impulse response $h(t)$ corresponding to a general bandpass filter

$$H(\omega) = A_h(\omega)e^{j\varphi_h(\omega)} \tag{9}$$

with double-sided bandwidth $2B_h$ centered at $\omega_h \geq B_h$ and intersecting the *support* of $X(\omega)$ (that is, where it is not zero), and amplitude and phase components $A_h(\omega)$ and $\varphi_h(\omega)$, respectively. Let $y(t)$ be the bandpass output of the system, and ω_0 be a reference frequency lying in the supports of $X(\omega)$ and $H(\omega)$ and satisfying condition (7) for both spectrums. Then it can be shown that the original bandpass system

$$y(t) = h(t) \circledast x(t) \quad \text{or} \quad Y(\omega) = H(\omega)X(\omega) \tag{10a}$$

is equivalent to the *LPE system*

$$\boxed{\tilde{y}(t) = \tfrac{1}{2}\tilde{h} \circledast \tilde{x}(t) \quad \text{or} \quad \tilde{Y}(\omega) = \tfrac{1}{2}\tilde{H}(\omega)\tilde{X}(t)(\omega)} \tag{10b}$$

where from (8c)

$$\boxed{\tilde{H}(\omega) = Z_h(\omega + \omega_0) = 2H(\omega + \omega_0)U(\omega + \omega_0)} \tag{11}$$

is the LPE filter referenced to ω_0.

As can be seen from Fig. 4(b), $\tilde{H}(\omega)$ can be asymmetrical about $\omega = 0$ in general, and hence will give rise to a complex impulse response

$$\tilde{h}(t) = p(t) + jq(t) \tag{12}$$

where the real part $p(t)$ and imaginary part $q(t)$ of $\tilde{h}(t)$ are called the *in-phase* and *quadrature* components, respectively. Note that in view of (12), we can also decompose $\tilde{H}(\omega)$ as

$$\tilde{H}(\omega) = P(\omega) + jQ(\omega) \tag{13}$$

where $P(\omega)$ and $Q(\omega)$ would represent the in-phase and quadrature components of $\tilde{H}(\omega)$, respectively, and can readily be shown to be given by

$$P(\omega) = \frac{1}{2}[\tilde{H}(\omega) + \tilde{H}^*(-\omega)],$$
$$Q(\omega) = \frac{1}{2j}[\tilde{H}(\omega) - \tilde{H}^*(-\omega)]. \tag{14}$$

Note that both of these filters will have even amplitude components and odd phase components since they correspond to real impulse responses.

We close this subsection with some useful results for our analysis whose derivation can be found in the Appendix.

i) Suppose the bandpass signal $x(t)$ described above is specialized to an amplitude and phase modulated signal given by

$$x(t) = x_p(t)\cos(\omega_0 t + \varphi_0) - x_q(t)\sin(\omega_0 t + \varphi_0) \tag{15a}$$

or

$$x(t) = A_x(t)\cos[\omega_0 t + \varphi_0 + \varphi_x(t)] \tag{15b}$$

where φ_0 is an arbitrary constant; $x_p(t), x_q(t), A_h(t)$, and $\varphi_x(t)$ are bandlimited signals with bandwidth $B \leq \omega_0$ and related by

$$|A_x(t)| = [x_p^2(t) + x_q^2(t)]^{1/2}, \quad \varphi_x(t) = \tan^{-1}\left[\frac{x_q(t)}{x_p(t)}\right] \tag{16a}$$

and

$$x_p(t) = A_x(t)\cos\varphi_x(t), \quad x_q(t) = A_x(t)\sin\varphi_x(t). \tag{16b}$$

Then the response $y(t)$ of the general bandpass filter in (9) to $x(t)$ in (15) is given by

$$\boxed{y(t) = \tfrac{1}{2}[\tilde{y}_p(t)\cos(\omega_0 t + \varphi_0) - \tilde{y}_q(t)\sin(\omega_0 t + \varphi_0)]} \tag{17a}$$

where $\tilde{y}_p(t)$ and $\tilde{y}_q(t)$ are formed by the following convolutions of $x_p(t)$ and $x_q(t)$ with the real components $p(t)$ and $q(t)$ of $\tilde{h}(t)$:

$$\boxed{\begin{aligned}\tilde{y}_p(t) &= x_p(t) \circledast p(t) - x_q(t) \circledast q(t)\\ \tilde{y}_q(t) &= x_q(t) \circledast p(t) + x_p(t) \circledast q(t).\end{aligned}} \tag{17b}$$

We can obtain equivalent convolutions with $A_x(t)$ and $\varphi_x(t)$ through the use of (16b) in (17b).

For the special case of (15b) in which

$$\varphi_x(t) \equiv \varphi_x = \text{constant} \tag{18}$$

we have that

$$\boxed{\begin{aligned}y(t) = \tfrac{1}{2}[&\tilde{y}_p(t)\cos(\omega_0 t + \varphi_0 + \varphi_x)\\ &- \tilde{y}_q(t)\sin(\omega_0 t + \varphi_0 + \varphi_x)]\end{aligned}} \tag{19a}$$

where

$$\boxed{\tilde{y}_p(t) = A_x(t) \circledast p(t), \quad \tilde{y}_q(t) = A_x(t) \circledast q(t).} \tag{19b}$$

ii) The output $y(t)$ of a general filter $H(\omega)$, expressed as in (9), to the input

$$x(t) = \cos(\omega_s t + \varphi_x), \quad \varphi_x = \text{constant} \tag{20}$$

is given by

$$\boxed{y(t) = h(t) \circledast x(t) = A_h(\omega_s)\cos[\omega_s t + \varphi_x + \varphi(\omega_s)]} \tag{21a}$$

or expressed in the frequency domain,

$$\begin{aligned} Y(\omega) &= H(\omega)X(\omega) = H(\omega)\mathcal{F}\{\cos(\omega_s t + \varphi_x)\} \\ &= H(\omega_s)e^{\jmath\varphi_x}\mathcal{F}\{\cos\omega_s t\} \end{aligned} \tag{21b}$$

where $\mathcal{F}\{\cdot\}$ represents the Fourier transform operator defined through

$$\mathcal{F}\{f(t)\} =: F(\omega) := \int_{-\infty}^{\infty} f(t)e^{\jmath\omega t}\,dt \tag{22}$$

for any function $f(t)$ for which the definite integral is well defined. A result similar to (21) would hold for the case of a sine function used instead for $x(t)$, noting the quadrature relation

$$\mathcal{F}\{\sin\omega_s t\} = -\jmath\mathcal{F}\{\cos\omega_s t\}. \tag{23}$$

2) DSB Cascade Model: Because the VNA utilizes a swept tone as its stimulus signal for probing a given DUT, we will take, without loss in generality,

$$u_1(t) = u(t) = \cos\omega_s t \tag{24}$$

in the cascaded FTD models in Fig. 3 where $\omega_s \geq 0$ is the probing frequency. The goal here is to calculate the output $z(t)$ as a modulated version of $u(t)$, thus allowing for the identification of the transmission response of the cascaded FTD's that is characterized by the product $H_1(\omega)H_2(\omega)$ or $\tilde{H}_1(\omega)\tilde{H}_2(\omega)$.

As a consequence of length constraints and so as not to be repetitious, we will only treat in detail the mathematical analysis of the baseband DSB method in this subsection. The analysis of the RF DSB method is simpler and quite analogous in form to that for the baseband version, so that a sketch of the arguments will suffice.

Referring to Fig. 3(a), the detailed model of FTD 1 is given in Fig. 2(b), while that for FTD 2 is presented in Fig. 2(d), with the appropriate subscripts applied to the various model quantities. Using (24) and Fig. 2(b), we see that

$$v_1(t) = \cos\omega_s t\cos(\omega_0 t + \varphi_{L1}) \tag{25}$$

will be the output of the multiplier. Note that $v_1(t)$ is in the form of $x(t)$ in (15b) with

$$A_x(t) = \cos\omega_s t, \quad \varphi_0 = 0, \quad \varphi_x(t) \equiv \varphi_{L1}. \tag{26}$$

Because the special case (18) for $\varphi_x(t)$ holds here, we have from (19) to (21a) and (26) that the output $y_1(t)$ of the bandpass filter $H_1(\omega)$ in terms of its LPE $\tilde{H}_1(\omega)$ is given by

$$y_1(t) = \tfrac{1}{2}[\tilde{y}_{1p}(t)\cos(\omega_0 t + \varphi_{L1}) - \tilde{y}_{1q}(t)\sin(\omega_0 t + \varphi_{L1})] \tag{27a}$$

where

$$\begin{aligned} \tilde{y}_{1p}(t) &= \cos\omega_s t \circledast p_1(t) = A_{p_1}(\omega_s)\cos[\omega_s t + \varphi_{p_1}(\omega_s)] \\ \tilde{y}_{1q}(t) &= \cos\omega_s t \circledast q_1(t) = A_{q_1}(\omega_s)\cos[\omega_s t + \varphi_{q_1}(\omega_s)] \end{aligned} \tag{27b}$$

and, in accordance with our convention (9), we have written

$$\begin{aligned} \tilde{H}_1(\omega) &= P_1(\omega) + \jmath Q_1(\omega) \\ &= A_{p_1}(\omega)e^{\jmath\varphi_{p_1}(\omega)} + \jmath A_{q_1}(\omega)e^{\jmath\varphi_{q_1}(\omega)} \end{aligned} \tag{27c}$$

which will also hold similarly for $\tilde{H}_2(\omega)$, below.

Moving on to FTD 2, we have that

$$u_2(t) = y_1(t). \tag{28}$$

Noting that (27a) is already in the form of (15a) with $x_p(t) = \frac{1}{2}\tilde{y}_{1p}(t), x_q(t) = \frac{1}{2}\tilde{y}_{1q}(t)$, and $\varphi_0 = \varphi_{L1}$, we conclude from (17), (27b), (28), and result i) of Section III-B1) that the output $v_2(t)$ of the second bandpass filter $H_2(\omega)$ is given by

$$v_2(t) = \tfrac{1}{2}[\tilde{v}_{2p}(t)\cos(\omega_0 t + \varphi_{L1}) - \tilde{v}_{2q}(t)\sin(\omega_0 t + \varphi_{L2})] \tag{29a}$$

where

$$\begin{aligned} \tilde{v}_{2p}(t) &= \tfrac{1}{2}[\tilde{y}_{1p}(t) \circledast p_2(t) - \tilde{y}_{1q}(t) \circledast q_2(t)] \\ &= \tfrac{1}{2}[A_{p_1p_2}\cos(\omega_s t + \varphi_{p_1p_2}) \\ &\quad - A_{q_1q_2}\cos(\omega_s t + \varphi_{q_1q_2})], \end{aligned} \tag{29b}$$

$$\begin{aligned} \tilde{v}_{2q}(t) &= \tfrac{1}{2}[\tilde{y}_{1q}(t) \circledast p_2(t) + \tilde{y}_{1p}(t) \circledast q_2(t)] \\ &= \tfrac{1}{2}[A_{q_1p_2}\cos(\omega_s t + \varphi_{q_1p_2}) \\ &\quad - A_{p_1q_2}\cos(\omega_s t + \varphi_{p_1q_2})] \end{aligned} \tag{29c}$$

and

$$\left.\begin{aligned} A_{kl} &:= A_k(\omega_s)A_l(\omega_s) \\ \varphi_{kl} &:= \varphi_k(\omega_s) + \varphi_l(\omega_s) \end{aligned}\right\}, \quad k,l \in \{p_1,p_2,q_1,q_2\}, \quad k \neq l. \tag{29d}$$

In anticipation of the upcoming SSB analysis, and for the sake of a more explicit statement of the frequency translation operation, we reexpress $v_2(t)$ in terms of the frequencies $\omega_0 \pm \omega_s$ using standard trigonometric product identities as follows:

$$\begin{aligned} v_2(t) = \tfrac{1}{8}[&A_{p_1p_2}\{\cos[(\omega_0+\omega_s)t + \varphi_{L1} + \varphi_{p_1p_2}] \\ &+ \cos[(\omega_0-\omega_s)t + \varphi_{L1} - \varphi_{p_1p_2}]\} \\ &- A_{q_1q_2}\{\cos[(\omega_0+\omega_s)t + \varphi_{L1} + \varphi_{q_1q_2}] \\ &+ \cos[(\omega_0-\omega_s)t + \varphi_{L1} - \varphi_{q_1q_2}]\} \\ &- A_{q_1p_2}\{\sin[(\omega_0+\omega_s)t + \varphi_{L1} + \varphi_{q_1p_2}] \\ &+ \sin[(\omega_0-\omega_s)t + \varphi_{L1} - \varphi_{q_1p_2}]\} \\ &- A_{p_1q_2}\{\sin[(\omega_0+\omega_s)t + \varphi_{L1} + \varphi_{p_1q_2}] \\ &+ \sin[(\omega_0-\omega_s)t + \varphi_{L1} - \varphi_{p_1q_2}]\}]. \end{aligned} \tag{30}$$

Finally, after passing $v_2(t)$ through the second ideal multiplier to arrive at $y_2(t)$, and filtering out the harmonics at $2\omega_0 \pm \omega_s$ with the ideal harmonic filter $H_o(\omega)$, assuming that

$$0 \le \omega_s < \frac{\omega_0}{2} \tag{31}$$

so that $2\omega_0 - \omega_s > \omega_0 + \omega_s$, we find that the output $z(t)$ of the cascaded DSB model is given by

$$\begin{aligned} z(t) = \tfrac{1}{16}\{ & A_{p_1p_2}[\cos(\omega_s t - \Delta\varphi_L + \varphi_{p_1p_2}) \\ & + \cos(\omega_s t + \Delta\varphi_L + \varphi_{p_1p_2})] \\ & - A_{q_1q_2}[\cos(\omega_s t - \Delta\varphi_L + \varphi_{q_1q_2}) \\ & + \cos(\omega_s t + \Delta\varphi_L + \varphi_{q_1q_2})] \\ & - A_{q_1p_2}[\sin(\omega_s t - \Delta\varphi_L + \varphi_{q_1p_2}) \\ & - \sin(\omega_s t + \Delta\varphi_L + \varphi_{q_1p_2})] \\ & - A_{p_1q_2}[\sin(\omega_s t - \Delta\varphi_L + \varphi_{p_1q_2}) \\ & - \sin(\omega_s t + \Delta\varphi_L + \varphi_{p_1q_2})]\} \end{aligned} \tag{32}$$

where

$$\boxed{\Delta\varphi_L := \varphi_{L2} - \varphi_{L1}} \tag{33}$$

and we have written the terms in $z(t)$ so as to match in parallel with the ones they were derived from in (30) (again with the upcoming SSB analysis in mind).

We now wish to compute the Fourier transform $Z(\omega) = Z(\omega_s)$ of $z(t)$ in (32) and express it as a product of the transmission response of the FTD pair and $\mathcal{F}\{\cos\omega_s t\}$, the Fourier transform of the original probing input tone. Using result i) of Section III-B), one can determine that

$$\begin{aligned} Z(\omega_s) = \tfrac{1}{16}[& (H^+_{p_1p_2} + H^-_{p_1p_2} - H^+_{q_1q_2} - H^-_{q_1q_2}) \\ & + \jmath(H^-_{q_1p_2} - H^+_{q_1p_2} + H^-_{p_1q_2} - H^+_{p_1q_2})]\mathcal{F}\{\cos\omega_s t\} \end{aligned} \tag{34a}$$

where we have defined the augmented LPE filters

$$\left.\begin{aligned} H^{\pm}_{kl} &:= H_{kl}e^{\pm\jmath\Delta\varphi_L} \\ H_{kl} &:= A_{kl}e^{\jmath\varphi_{kl}} \end{aligned}\right\}, \qquad k,l \in \{p_1,p_2,q_1,q_2\}, \quad k \ne l \tag{34b}$$

and A_{kl}, φ_{kl}, and $\Delta\varphi_L$ are as defined in (29d) and (33). From (34) we conclude that the measured transfer function $M_{\rm I}(\omega_s)$ through the test system is given by

$$\begin{aligned} M_{\rm I}(\omega_s) &:= \frac{Z(\omega_s)}{\mathcal{F}\{\cos\omega_s t\}} \\ &= \tfrac{1}{16}\{[H_{p_1p_2} - H_{q_1q_2} + \jmath(H_{q_1p_2} + H_{p_1q_2})]e^{-\jmath\Delta\varphi_L} \\ &\quad + [H_{p_1p_2} - H_{q_1q_2} - \jmath(H_{q_1p_2} + H_{p_1q_2})]e^{\jmath\Delta\varphi_L}\}. \end{aligned} \tag{35}$$

Now from (14), (29d), and (34b), it follows that

$$\begin{aligned} H_{p_1p_2} - H_{q_1q_2} &= P_1P_2 - Q_1Q_2 \\ &= \tfrac{1}{2}[\tilde{H}_1(\omega_s)\tilde{H}_2(\omega_s) + \tilde{H}_1^*(-\omega_s)\tilde{H}_2^*(-\omega_s)] \\ H_{q_1p_2} - H_{p_1q_2} &= Q_1P_2 - P_1Q_2 \\ &= \tfrac{1}{2\jmath}[\tilde{H}_1(\omega_s)\tilde{H}_2(\omega_s) - \tilde{H}_1^*(-\omega_s)\tilde{H}_2^*(-\omega_s)] \end{aligned} \tag{36}$$

so that $M_{\rm I}(\omega_s)$ in (35) can be more simply expressed by

$$\boxed{\begin{aligned} M_{\rm I}(\omega_s) = \tfrac{1}{16}[& \tilde{H}_1(\omega_s)\tilde{H}_2(\omega_s)e^{-\jmath\Delta\varphi_L} \\ & + \tilde{H}_1^*(-\omega_s)\tilde{H}_2^*(-\omega_s)e^{\jmath\Delta\varphi_L}]. \end{aligned}} \tag{37}$$

Because the desired product filter $\tilde{H}_1(\omega_s)\tilde{H}_2(\omega_s)$ is generally asymmetric, it is clear from (37) that one measurement will not suffice to de-embed it. However, by making a second measurement of the overall transfer function with the difference angle $\Delta\varphi_L$ in (33) shifted by $+(\pi/2)$—which would correspond to adjusting the phase shifter on the second LO arm by $+(\pi/2)$ (see Fig. 1)—we can retrieve $\tilde{H}_1(\omega_s)\tilde{H}_2(\omega_s)$ as needed. Indeed, applying the transformation $\Delta\varphi_L \to \Delta\varphi_L + \pi/2$ to (37), and using the fact $e^{\pm\jmath(\pi/2)} = \pm\jmath$, we conclude that

$$\boxed{\begin{aligned} M_{\rm II}(\omega_s) &:= M_{\rm I}(\omega_s)|_{\Delta\varphi_L \to \Delta\varphi_L + (\pi/2)} \\ &= \tfrac{\jmath}{16}[\tilde{H}_1^*(-\omega_s)\tilde{H}_2^*(-\omega_s)e^{\jmath\Delta\varphi_L} \\ &\quad - \tilde{H}_1(\omega_s)\tilde{H}_2(\omega_s)e^{-\jmath\Delta\varphi_L}]. \end{aligned}} \tag{38}$$

Finally, by combining $M_{\rm I}(\omega_s)$ with a $+(\pi/2)$-shifted version of $M_{\rm II}(\omega_s)$, that is, $+\jmath M_{\rm II}(\omega_s)$, we see from (37) and (38) that

$$M_{\rm I}(\omega_s) + \jmath M_{\rm II}(\omega_s) = \tfrac{1}{8}e^{-\jmath\Delta\varphi_L}\tilde{H}_1(\omega_s)\tilde{H}_2(\omega_s) \tag{39}$$

so that

$$\begin{aligned} \tilde{H}_1(\omega_s)\tilde{H}_2(\omega_s) = & 8e^{\jmath\Delta\varphi_L}[M_{\rm I}(\omega_s) + \jmath M_{\rm II}(\omega_s)], \\ & 0 \le \omega_s < \tfrac{\omega_0}{2}. \end{aligned} \tag{40}$$

In order to obtain this product for $\omega_s \le 0$, we use the fact that $M_{\rm I}$ and $M_{\rm II}$ must correspond to real impulse responses and hence must satisfy the symmetry property

$$M_i(\omega_s) = M_i^*(-\omega_s), \qquad i = \text{I or II}. \tag{41}$$

We thus conclude from (40) and (41) that

$$\begin{aligned} \tilde{H}_1(\omega_s)\tilde{H}_2(\omega_s) = & 8e^{\jmath\Delta\varphi_L}[M_{\rm I}^*(-\omega_s) + \jmath M_{\rm II}^*(-\omega_s)], \\ & -\tfrac{\omega_0}{2} < \omega_s \le 0. \end{aligned} \tag{42}$$

Observe from (40) and (42) that the product response is uniquely determined from the measurements except for the fixed phase offset $\Delta\varphi_L$ given in (33). This offset is essentially of no consequence to performance evaluations, since it is the shape of the phase versus frequency that is important in these considerations.

We now finally define the *LPE DSB FTD transmission response* $T^{\rm DSB}(\omega)$ by

$$\boxed{T^{\rm DSB}(\omega) := \tfrac{1}{4}\tilde{H}(\omega).} \tag{43}$$

We comment here that the $\frac{1}{4}$-factor in (43) derives from the $\frac{1}{2}$-factor normally associated with LPE systems [see (10b)], and the $\frac{1}{2}$-factor coming from the perfect spectral splitting manifested in the ideal multiplier output.

Hence, by (40) and (42) we find that

$$\boxed{\begin{aligned}\Pi^{\mathrm{DSB}}(\omega_s) &:= T_1^{\mathrm{DSB}}(\omega_s)T_2^{\mathrm{DSB}}(\omega_s)\\ &= \begin{cases}\frac{1}{2}\, e^{\jmath\Delta\varphi_L}[M_{\mathrm{I}}^*(-\omega_s) + \jmath M_{\mathrm{II}}^*(-\omega_s)], \\ \qquad -\frac{\omega_0}{2} < \omega_s \le 0\\ \frac{1}{2}\, e^{\jmath\Delta\varphi_L}[M_{\mathrm{I}}(\omega_s) + \jmath M_{\mathrm{II}}(\omega_s)], \\ \qquad 0 \le \omega_s < \frac{\omega_0}{2}\end{cases}\end{aligned}} \tag{44}$$

which will be used in the de-embedding procedure outlined in Section III-C, below.

For the RF DSB method, we refer to Fig. 3(b) and note that the bandpass filters that characterize the two FTD's lie external to the ideal translation and harmonic filtering that takes place between them. As a result of this observation, and through the use of simple spectral arguments, one can demonstrate that only one measured input/output *bandpass* transfer function $M(\omega_s)$ is needed here, and it will be essentially the product of the bandpass FTD filters $H_i(\omega_s), i = 1, 2$, except for factors of $\frac{1}{2}$ corresponding to energy losses from the two ideal frequency translations. It can be shown that the LPE DSB FTD transmission response is again given by (43), whereas the product LPE response $\Pi^{\mathrm{DSB}}(\omega_s)$ needed for de-embedding is instead given by

$$\boxed{\begin{aligned}\Pi^{\mathrm{DSB}}(\omega_s) &:= T_1^{\mathrm{DSB}}(\omega_s)T_2^{\mathrm{DSB}}(\omega_s)\\ &= \tfrac{1}{2}\,\tilde{M}(\omega_s)e^{\jmath\Delta\varphi_L},\\ &\qquad -\tfrac{\omega_0}{2} < \omega_s \le \tfrac{\omega_0}{2}\end{aligned}} \tag{45}$$

where $\tilde{M}(\omega_s)$ represents the LPE of $M(\omega_s)$ that will generally *not* be symmetrical with respect to $\omega_s = 0$.

3) SSB Cascade Model Because many of the SSB results will readily follow from the general analysis done for the baseband DSB method just presented, our exposition here will be abridged. We will cover the USB and LSB cases separately.

USB Case: For the sake of reference, the intermediate signals in the cascaded SSB model are as follows. Referring to Fig. 2(a), the output $v_1(t)$ of the ideal multiplier will again be given by (25), while the output of the bandpass filter $H_1(\omega)$ will again be given by (27). Using standard product trigonometric identities, $w_1(t)$ can be re-expressed to show the frequency translation explicitly as

$$\begin{aligned}w_1(t) = &\frac{A_{p_1}}{4}\,\{\cos[(\omega_0+\omega_s)t + \varphi_{L1} + \varphi_{p_1}]\\ &+ \cos[(\omega_0-\omega_s)t + \varphi_{L1} - \varphi_{p_1}]\}\\ &- \frac{A_{q_1}}{4}\,\{\sin[(\omega_0+\omega_s)t + \varphi_{L1} + \varphi_{q_1}]\\ &- \sin[(\omega_0-\omega_s)t + \varphi_{L1} - \varphi_{q_1}]\}\end{aligned} \tag{46}$$

where we have dropped the ω_s-argument of the amplitudes A_i and phases φ_i $(i = p_1, q_1)$ of $P_1(\omega)$ and $Q_1(\omega)$ for simplicity. Applying the brickwall filter $H_{b1}(\omega)$ in (3a) to $w_1(t)$ in (46), we have the output $y_1(t)$ of FTD 1:

$$\begin{aligned}y_1(t) = &\tfrac{1}{4}\{A_{p_1}\cos[(\omega_0+\omega_s)t + \varphi_{L1} + \varphi_{p_1}]\\ &- A_{q_1}\sin[(\omega_0+\omega_s)t + \varphi_{L1} + \varphi_{q_1}]\}.\end{aligned} \tag{47}$$

Moving on to FTD 2 [which is LSB; see Fig. 2(c)], we have that

$$u_2(t) = y_1(t). \tag{48}$$

At this point, we make an important simplifying observation that will allow us to derive the output $v_2(t)$ of $H_2(\omega)$ of the cascaded pair immediately from the DSB case, as well as obtaining the signals $w_2(t)$ and $z(t)$. Note that in the cascaded SSB model, the bandpass filter $H_1(\omega)$ is followed by the brickwall filter $H_{b1}(\omega)$, followed finally by the bandpass filter $H_2(\omega)$. By linearity, the output of this sequence of filters is identical to that of the sequence $H_1(\omega), H_2(\omega)$, and $H_{b1}(\omega)$. We thus just need to apply $H_{b1}(\omega)$ given by (3a) to the result $v_2(t)$ in (30) to arrive at

$$\begin{aligned}v_2(t) = &\tfrac{1}{8}\{A_{p_1p_2}\cos[(\omega_0+\omega_s)t + \varphi_{L1} + \varphi_{p_1p_2}]\\ &- A_{q_1q_2}\cos[(\omega_0+\omega_s)t + \varphi_{L1} + \varphi_{q_1q_2}]\\ &- A_{q_1p_2}\sin[(\omega_0+\omega_s)t + \varphi_{L1} + \varphi_{q_1p_2}]\\ &- A_{p_1q_2}\sin[(\omega_0+\omega_s)t + \varphi_{L1} + \varphi_{p_1q_2}]\}.\end{aligned} \tag{49}$$

After passing $v_2(t)$ through the second ideal multiplier to arrive at $w_2(t)$, filtering with the second brickwall filter $H_{b2}(\omega)$ [which is also given by (3b)] will produce $y_2(t)$. Finally, filtering $y_2(t)$ with the same harmonic filter $H_o(\omega)$ as in the DSB case [but without condition (31) needed], (32) gives

$$\begin{aligned}z(t) = &\tfrac{1}{16}[A_{p_1p_2}\cos(\omega_s t - \Delta\varphi_L + \varphi_{p_1p_2})\\ &- A_{q_1q_2}\cos(\omega_s t - \Delta\varphi_L + \varphi_{q_1q_2})\\ &- A_{q_1p_2}\sin(\omega_s t - \Delta\varphi_L + \varphi_{q_1p_2})\\ &- A_{p_1q_2}\sin(\omega_s t - \Delta\varphi_L + \varphi_{p_1q_2})]\end{aligned} \tag{50}$$

where $\Delta\varphi_L$ is as in (33). It follows that $Z(\omega_s)$ would be as in (34), but with the H_{kl}^+ terms removed. The measured transfer function $M_{\mathrm{I}}(\omega_s) =: M(\omega_s)$ would thus in this case be given by

$$\boxed{M(\omega_s) = \tfrac{1}{16}\,\tilde{H}_1(\omega_s)\tilde{H}_2(\omega_s)e^{-\jmath\Delta\varphi_L}} \tag{51}$$

where we have used (37). In view of the additional brickwall filter $H_{b2}(\omega)$ of (3b) that is contained in the FTD here, the analog of (44) is

$$\boxed{\begin{aligned}\Pi^{\mathrm{USB}}(\omega_s) &= T_1^{\mathrm{USB}}(\omega_s)T_2^{\mathrm{USB}}(\omega_s)\\ &= M(\omega_s)e^{\jmath\Delta\varphi_L}, \qquad \omega_s \ge 0\end{aligned}} \tag{52}$$

where the LPE USB FTD transmission response is defined as

$$\boxed{T^{\mathrm{USB}}(\omega) := \tfrac{1}{4}\tilde{H}(\omega)U(\omega)} \tag{53}$$

and $U(\omega)$ is the unit step function given in (6). The product $\Pi^{\mathrm{USB}}(\omega_s)$ is suitable for usage in the de-embedding procedure of Section III-C, below. Hence only one measurement is needed in this case, in contrast to the previous DSB class.

LSB Case: In an entirely similar manner, the signal waveforms for FTD 1 of the LSB case would be as follows: $v_1(t)$ as in (25), $w_1(t)$ as in (27) and (46), while $y_1(t)$ would be as in (47) with $\omega_0 + \omega_s$ replaced by $\omega_0 - \omega_s$ and φ_i by $-\varphi_i$ $(i = p_1, q_1)$. For FTD 2, we would have that (48) holds again, $v_2(t)$ is as in (49) with $\omega_0 + \omega_s$ replaced by $\omega_0 - \omega_s$ and φ_{kl} by $-\varphi_{kl}$, and $z(t)$ given by

$$\begin{aligned} z(t) = \tfrac{1}{16}[&A_{p_1p_2}\cos(\omega_s t + \Delta\varphi_L + \varphi_{p_1p_2}) \\ &- A_{q_1q_2}\cos(\omega_s t + \Delta\varphi_L + \varphi_{q_1q_2}) \\ &+ A_{q_1p_2}\sin(\omega_s t + \Delta\varphi_L + \varphi_{q_1p_2}) \\ &- A_{p_1q_2}\sin(\omega_s t + \Delta\varphi_L + \varphi_{p_1q_2})] \end{aligned} \tag{54}$$

where the harmonic filter $H_o(\omega_s)$ is as before with condition (31) replaced by

$$0 \le \omega < \omega_0 \tag{55}$$

so that $2\omega_0 - \omega_s > \omega_s$ instead, and $\Delta\varphi_L$ is as in (33). Here $Z(\omega_s)$ would be as in (34) with the H_{kl}^- terms deleted. The measured transfer function $M(\omega_s)$ in this case is given by

$$\boxed{M(\omega_s) = \tfrac{1}{16}\hat{H}_1^*(-\omega_s)\hat{H}_2^*(-\omega_s)e^{j\Delta\varphi_L}.} \tag{56}$$

Using the symmetry property (41) and proceeding in a manner similar to that used for the USB case, the product response becomes

$$\boxed{\begin{aligned} \Pi^{\mathrm{LSB}}(\omega_s) &= T_1^{\mathrm{LSB}}(\omega_s)T_2^{\mathrm{LSB}}(\omega_s) \\ &= M^*(-\omega_s)e^{j\Delta\varphi_L}, \qquad -\omega_0 < \omega_s \le 0 \end{aligned}} \tag{57}$$

where the LPE LSB FTD transmission response is defined as

$$\boxed{T^{\mathrm{LSB}}(\omega) = \tfrac{1}{4}\hat{H}(\omega)U(-\omega).} \tag{58}$$

C. FTD Transmission Response De-Embedment

We will now detail the de-embedding procedure for determining the LPE transmission response of a given FTD DUT. Recall that all LPE responses have been referenced to the LO frequency ω_0. For those cases in which the sweep is bandpass in nature and centered at ω_u, the resulting LPE responses will also be bandpass and centered at ω_u. In order to place all LPE responses at a common dc center frequency, we introduce an additional frequency shift of ω_u, as can be seen in (1). Thus, to de-embed this response, we first define

$$R(\omega) := \begin{cases} 20\log_{10} A(\omega_u) \text{ for the amplitude} \\ \varphi(\omega_u) \text{ for the phase} \end{cases} \tag{59}$$

where $T(\omega_u) = A(\omega)e^{j\varphi(\omega)}$ and $T(\omega)$ generically denotes the LPE FTD transmission response for any of the sideband cases given by (43), (53), and (58). Note that the product LPE transmission response $\Pi(\omega) = T_1(\omega)T_2(\omega)$ will thus obey the relation

$$R_\Pi(\omega) = R_1(\omega) + R_2(\omega) \tag{60}$$

for both the amplitude (dB) and the phase (degrees). Assume that three product transmission responses have been obtained as outlined in Section III-B2) and -B3) for three FTD cascades of three distinct FTD's of the same sideband type, denoted by DUT, TM1 (Test Mixer 1), and TM2 (Test Mixer 2). We will add the superscript "+/−" to $R(\omega)$ to represent the upconversion/downconversion response since these will only be equal if the FTD has reciprocal frequency response characteristics. Using the measured results described in Sections II-A and II-B in (44), (45), (52), or (57), and noting property (60), we arrive at the following relations:

$$\begin{aligned} R_{\mathrm{DUT}}^+ + R_{\mathrm{TM1}}^- &= R_A(\omega) \\ R_{\mathrm{TM1}}^+ + R_{\mathrm{DUT}}^- &= R_{A'}(\omega) \\ R_{\mathrm{DUT}}^+ + R_{\mathrm{TM2}}^- &= R_B(\omega) \\ R_{\mathrm{TM2}}^+ + R_{\mathrm{DUT}}^- &= R_{B'}(\omega) \\ R_{\mathrm{TM1}}^+ + R_{\mathrm{TM2}}^- &= R_C(\omega) \\ R_{\mathrm{TM2}}^+ + R_{\mathrm{TM1}}^- &= R_{C'}(\omega) \end{aligned} \tag{61}$$

where $R_X(\omega)$ corresponds to $\Pi_X(\omega)$ according to (59), $X = A, A', B, B', C, C'$.

If we assume only one FTD is reciprocal, say TM1, then $R_{\mathrm{TM1}}^+ = R_{\mathrm{TM1}}^- =: R_{\mathrm{TM1}}$. In this case, only three of the relations in (61) can be used simultaneously to solve for the DUT response:

$$R_{\mathrm{DUT}}^+ = \tfrac{1}{2}[R_A + R_B - R_C] \tag{62a}$$

when used as an upconverter, and

$$R_{\mathrm{DUT}}^- = \tfrac{1}{2}[R_{A'} + R_{B'} - R_{C'}] \tag{62b}$$

when used as a downconverter. Note that if TM2 was the only reciprocal FTD, a different set of relations in (61) would then be chosen to arrive at

$$R_{\mathrm{DUT}}^+ = \tfrac{1}{2}[R_A + R_B - R_{C'}] \tag{63a}$$

$$R_{\mathrm{DUT}}^- = \tfrac{1}{2}[R_{A'} + R_{B'} - R_C]. \tag{63b}$$

If TM1 and TM2 are both reciprocal FTD's, then $R_C = R_{C'}$. As a result, both (62) and (63) provide valid solutions for $R_{\mathrm{DUT}}^\pm$. Finally, if all three FTD's are reciprocal, then the valid solutions already provided by (62) and (63) will be augmented by the following:

$$R_{\mathrm{DUT}}^+ = \tfrac{1}{2}[R_A + R_{B'} - R_C] \tag{64a}$$

$$R_{\mathrm{DUT}}^- = \tfrac{1}{2}[R_{A'} + R_B - R_C] \tag{64b}$$

$$R_{\mathrm{DUT}}^+ = \tfrac{1}{2}[R_A + R_{B'} - R_{C'}] \tag{64c}$$

$$R_{\mathrm{DUT}}^- = \tfrac{1}{2}[R_{A'} + R_B - R_{C'}]. \tag{64d}$$

Since $R_{\mathrm{DUT}}^+ = R_{\mathrm{DUT}}^- = R_{\mathrm{DUT}}$ in this case, there will be eight valid solutions for the LPE DUT response which has been previously presented as (1). Note that the phase offset of (33) is not included in (1), as is evident from (1), (45), (52), and (57), and the discussion in Sections II-A and -B for the SSB and RF DSB method cases; and (2) by comparing (2) and (44) for the baseband DSB method.

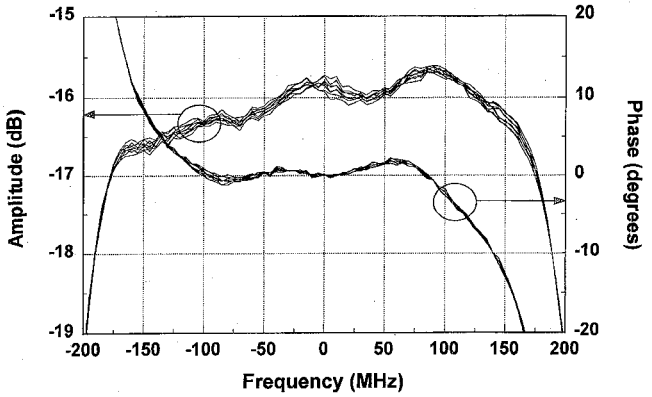

Fig. 5. Eight calculated VNA amplitude and phase responses for a 20 to 8 GHz SSB downconverter. The extremely close agreement of the measurements indicates the degree of repeatability of the SSB technique, and the frequency response reciprocity of all three FTD's used.

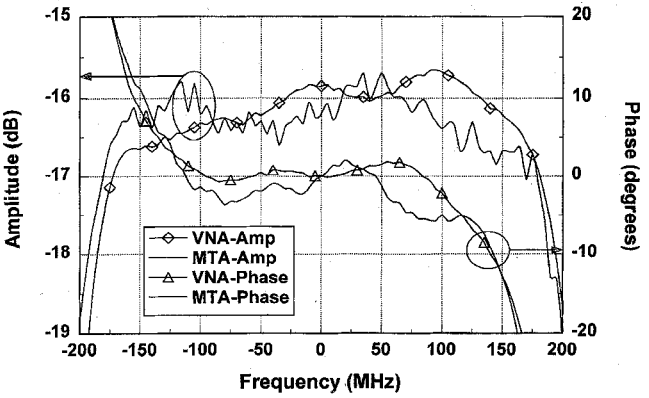

Fig. 6. Comparison of the average of the eight calculated VNA amplitude and phase responses in Fig. 5 with those measured directly with the MTA.

IV. Measurement Results

This section of the paper provides measured results for both SSB and DSB FTD's. The validation of the VNA technique is demonstrated for DUT's which are typical of those used in microwave communication systems. Validation of the technique is demonstrated with SSB FTD's by comparing results with another measurement technique using an MTA. Since they are the only known techniques for complete, absolute frequency response characterization of SSB FTD's, they are compared in terms of measurement accuracy, complexity, and applicability. Validation of the baseband DSB method is demonstrated by determining the response of two DUT's differing only by the addition of a bandpass filter and comparing their difference with a nonfrequency translating VNA measurement of the same bandpass filter alone. The RF DSB method is in turn verified by showing its close agreement with the results from the baseband DSB method.

A. SSB Downconverter Measurement

To demonstrate SSB FTD measurements, a 20 to 8 GHz downconverter was characterized. Measurements were performed with an HP 8510C VNA using a full two-port calibration. Low-side LO injection was used with a frequency of 12 GHz. The measurement bandwidth was 500 MHz, using 101 frequency points. At each frequency point, an averaging factor of eight was implemented and no data smoothing was applied. For the test mixers, two triple-balanced mixers (Watkins-Johnson Model WJ-MZ5010C) with a 1.0 to 15.0 GHz IF and a 2.0 to 26.0 GHz RF/LO were used. The eight calculated responses for both the amplitude and phase are shown over a 400 MHz bandwidth in Fig. 5. The tight grouping between response curves indicates that the DUT and both test mixers have reciprocal frequency response characteristics. Therefore the downconverter can also be used as an upconverter with the same frequency response. In this case, the most accurate response for the downconverter can be obtained by averaging the eight results shown.

B. SSB Measurement Validation

To validate the SSB FTD measurements, the same 20 to 8 GHz frequency converter was characterized using the MTA technique [3]. In the MTA measurements, the envelope delay technique was used with 2.5 MHz frequency modulation. The measurement procedure has been automated in an IBASIC program available from Hewlett-Packard (see [3]). The calibration procedure requires only a through path for normalization. The accuracy is therefore limited in comparison to the network analyzer approach where full error correction is used. For consistency, the measurements were performed using the same calibration frequency range and amount of averaging as was used in the VNA measurements. Measurements obtained from the MTA were compared with the average of the eight calculations from the VNA as shown in Fig. 6. It is clear that additional trace averaging could have been used to enhance noise reduction in the MTA measurements. This improvement would only be obtained at the expense of increased measurement time. The agreement between the amplitude and phase response curves was found to be within 1.15 dB and 6.14°, respectively, over the 400 MHz band. The difference in ripple structure between the measurement curves is primarily due to the inability of the MTA technique to remove the effects of VSWR interaction at the measurement ports.

C. DSB Downconverter Measurement

To demonstrate DSB FTD measurements, a 20 GHz-to-baseband downconverter (Watkins-Johnson WJ-M52C Mixer) was characterized. Two additional WJ-M52C devices were used as test mixers. As discussed earlier, the VNA measurement can be performed at either the higher (RF) or lower (baseband) input/output frequency range of the FTD's. For completeness, measurement of the FTD under test was carried out using both DSB methods. The measurements were performed with an HP 8510C VNA using full two-port calibrations. For the RF method, the VNA sweep frequency range for the three required measurements was 18.0 to 22.0 GHz using 401 points. For the baseband method, the VNA sweep frequency range for the six required measurements was 0.05 to 2.05 GHz using 201 points. An averaging factor of eight with no data smoothing was applied for both test configurations. A comparison of the calculated responses of the baseband and RF test methods is shown in Figs. 7 and 8, respectively. The good agreement between the curves indicates

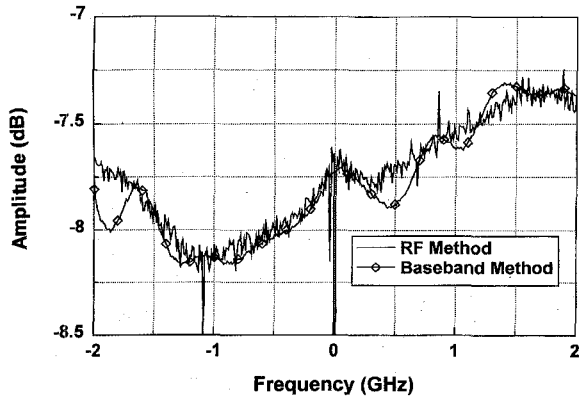

Fig. 7. Amplitude response comparison of the RF and baseband DSB measurement techniques for a 20 GHz-to-baseband downconverter. The close agreement of the curves indicates the consistency of the two approaches.

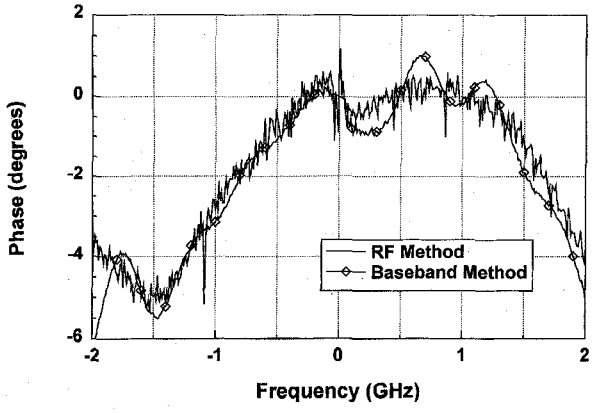

Fig. 8. Phase response comparison for the downconverter in Fig. 7. In this case, the resulting de-embedded phases were realigned by subtracting out the starting LO phase offsets. Again, the consistency of the two DSB techniques is borne out by the close agreement.

that both test methods provide valid results for DSB FTD's. Upon closer inspection, the RF method results are seen to contain a significant amount of additional broadband noise and are also clearly more prone to spurious noise spikes. The small amount of ripple found for the baseband characterization is a result of VSWR interaction and can be reduced by increasing the amount of attenuation at the mixer ports. We have found that with a suitable choice of mixer port attenuation, the baseband method provides the more accurate results for most DSB FTD's.

D. DSB Measurement Validation

A special validation test was devised here since there was no alternative method known to measure DSB FTD's. A DSB FTD with a 20 GHz LO was characterized with the baseband DSB technique and then the same FTD was re-characterized with a known linear network on its output. The second FTD response should be equal to the sum of the first FTD response and the known added linear network response. The ports of the FTD and linear network must be well matched, otherwise VSWR interaction will introduce significant measurement error. For the DSB validation measurement, the DUT was a DSB double-balanced mixer (ST Microwave Model MX1026C) and

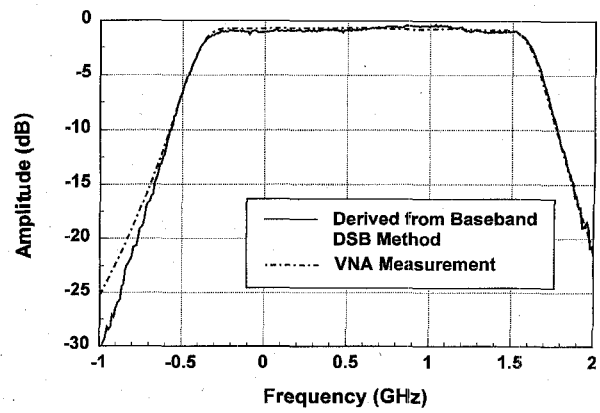

Fig. 9. Amplitude response of a K&L 5FV10-20600/T2000-0/0 bandpass filter derived from baseband DSB measurements compared to a direct VNA measurement. The close agreement serves to validate the baseband DSB measurement technique.

the linear network was a bandpass filter (K&L Microwave Model 5FV10-20600/T2000) with a center frequency of 20.6 GHz and a 3 dB bandwidth of 2.0 GHz.

The above measurements were performed and the filter response was derived by subtraction of the two responses. This derived response was then compared to the direct VNA measurement of the filter alone. The agreement between the derived and direct measurement is shown in Figs. 9 and 10 for the amplitude and phase, respectively, and serves to validate the technique. The results also validate the technique for asymmetric FTD's (note the 600 MHz offset corresponding to the difference between the LO and filter center frequencies). Observe that the derived response is the algebraic combination of twelve separate VNA measurements; six for both of the times the VNA technique was applied. Despite the build-up of random and systematic errors caused by combining twelve measurements, the agreement between the derived and direct measurement is good, except on the low frequency skirt of the filter. This disagreement is caused by the frequency offset of the filter bandcenter relative to the LO. This frequency offset causes the lower frequency skirt to fold on top of passband frequencies at baseband. Hence, at baseband, small amplitude signals from the lower frequency skirt interfere coherently with large amplitude signals from the filter passband. Small errors in the measurement of the large amplitude signals cause large errors in the measurement of the small signals. This indicates a limitation of the baseband VNA technique applied to DSB FTDs: the accuracy is reduced if the difference between sidebands is more than about 10 dB. Together with the previous comparisons presented in Section IV-C, these tests constitute a complete validation of both DSB characterization methods.

V. Conclusion

We have described a new method of obtaining the transmission response of FTD's. Both SSB and DSB FTD's can be characterized with accuracies approaching those of VNA measurements of non-FTD's. The technique test configuration has been presented along with general FTD measurement precautions. A complete detailed mathematical treatment of

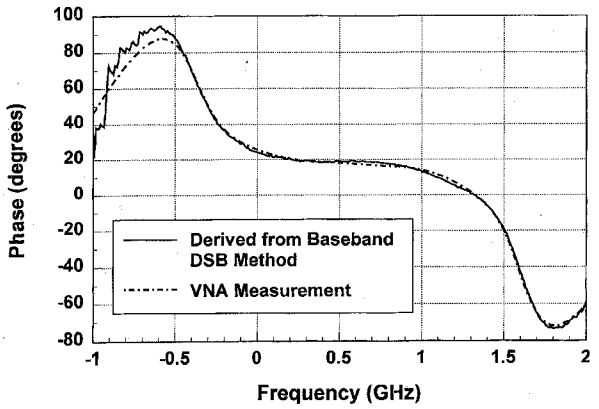

Fig. 10. Phase response of the same bandpass filter as in Fig. 9. Again we observe a close agreement between the derived and direct measurement of the response, providing further validation of the baseband DSB technique.

the technique has been presented using the concept of low-pass equivalent signals and systems. The validation and accuracy of the technique has been demonstrated with results for both SSB and DSB frequency converters operating at 20 GHz. Measurements were compared with the MTA technique for SSB FTD's and with nonfrequency-translating components for DSB FTD's.

APPENDIX
DERIVATION OF RESULTS i) AND ii) IN SECTION III-B

i) Given the general amplitude and phase modulated signal in (15) where the modulation signals are bandlimited as specified there. By trigonometric identities, (15b) can be expanded to

$$x(t) = A_x(t)\cos\varphi_x(t)\cos(\omega_0 t + \varphi_0) - A_x(t)\sin\varphi_x(t)\sin(\omega_0 t + \varphi_0) \tag{A.1}$$

from which (16b) follows. From (15a), we see that

$$X(\omega) = \tfrac{1}{2}\{[X_p(\omega-\omega_0) + jX_q(\omega-\omega_0)]e^{j\varphi_0} + [X_p(\omega+\omega_0) + jX_q(\omega+\omega_0)]e^{-j\varphi_0}\}. \tag{A.2}$$

From the first relation in (5), (A.2) becomes

$$Z_x(\omega) = [X_p(\omega-\omega_0) + jX_q(\omega-\omega_0)]e^{j\varphi_0} \tag{A.3}$$

since $X_i(\omega-\omega_0) = 0$ for $\omega < 0$ and $X_i(\omega+\omega_0) = 0$ for $\omega > 0, i = p, q$, using the assumption that $X_i(\omega) = 0$ for $|\omega| > \omega_0$. From (4a) and (A.3), we conclude that

$$\begin{aligned}\hat{x}(t) &= \mathrm{Im}[z_x(t)] = \mathrm{Im}\{[x_p(t) + jx_q(t)]e^{j(\omega_0 t+\varphi_0)}\} \\ &= x_p(t)\sin(\omega_0 t + \varphi_0) + x_q(t)\cos(\omega_0 t + \varphi_0)\end{aligned} \tag{A.4}$$

where Im(·) means the imaginary part. By (4a), (15a), and (A.4), the preenvelope of $x(t)$ is given by

$$z_x(t) = x(t) + j\hat{x}(t) = [x_p(t) + jx_q(t)]e^{j(\omega_0 t+\varphi_0)} \tag{A.5}$$

so that by (8b),

$$\tilde{x}(t) = [x_p(t) + jx_q(t)]e^{j\varphi_0}. \tag{A.6}$$

By (4a), (8a), (10b), (12), and (A.6), we find that

$$y(t) = \mathrm{Re}[z_y(t)] = \mathrm{Re}[\tilde{y}(t)e^{j\omega_0 t}] \tag{A.7}$$

where Re(·) means the real part, and

$$\begin{aligned}\tilde{y}(t) &= \tfrac{1}{2}\tilde{h}(t) \circledast \tilde{x}(t) \\ &= \tfrac{1}{2}[p(t) + jq(t)] \circledast [x_p(t) + jx_q(t)]e^{j\varphi_0} \\ &= \tfrac{1}{2}e^{j\varphi_0}\{[x_q(t) \circledast p(t) - x_q(t) \circledast q(t)] \\ &\quad + j[x_q(t) \circledast p(t) + x_p(t) \circledast q(t)]\}.\end{aligned} \tag{A.8}$$

Putting (A.8) in (A.7) gives (17).

The special case (19) follows from the general result by noting that $x(t)$ in (15b) with condition (18) holding is a special case of $x(t)$ in (15a) with

$$x_p(t) = A_x(t), \quad \varphi_0 = \varphi_0 + \varphi_x, \quad x_q(t) \equiv 0. \tag{A.9}$$

Putting (A.9) into (17) immediately gives (19).

ii) Let $x(t)$ be as in (20) and $\mathcal{F}$ and $\mathcal{F}^{-1}$ be the forward and reverse Fourier transform operators. Then for a general filter $H(\omega)$, the output is given by

$$\begin{aligned}y(t) &= h(t) \circledast x(t) = \mathcal{F}^{-1}\{H(\omega)X(\omega)\} \\ &= \mathcal{F}^{-1}\{H(\omega)\tfrac{1}{2}[e^{j\varphi_x}\delta(\omega-\omega_s) + e^{-j\varphi_x}\delta(\omega+\omega_s)]\} \\ &= \mathcal{F}^{-1}\{\tfrac{1}{2}[H(\omega_s)e^{j\varphi_x}\delta(\omega-\omega_s) \\ &\quad + H(-\omega_s)e^{-j\varphi_x}\delta(\omega+\omega_s)]\} \\ &= \tfrac{1}{2}[H(\omega_s)e^{j\varphi_x}e^{j\omega_s t} + H^*(\omega_s)e^{-j\varphi_x}e^{-j\omega_s t}] \\ &= \mathrm{Re}[H(\omega_s)e^{j\varphi_x}e^{j\omega_s t}] \\ &= \mathrm{Re}\{A(\omega_s)e^{j[\omega_s t+\varphi_x+\varphi(\omega_s)]}\}\end{aligned} \tag{A.10}$$

from which (21a) follows. Relation (21b) follows from the Fourier transform property

$$\mathcal{F}\{f(t+t_0)\} = e^{j\omega t_0}F(\omega) \tag{A.11}$$

rewriting the argument of the cosine function as follows:

$$\omega_s t + \varphi_x = \omega_s\left(t + \frac{\varphi_x}{\omega_s}\right) \Rightarrow t_0 = \frac{\varphi_x}{\omega_s}$$

taking $f(t) = \cos\omega_s t$ and recalling the sifting property of delta functions [that is, $f(t)\delta(t-t_0) = f(t_0)\delta(t-t_0)$]. For result (23), we have from the last relation in (21b) with $H(\omega) \equiv 1$ and $\omega = \omega_s$

$$\mathcal{F}\{\cos(\omega_s t + \varphi_x)\} = e^{j\varphi_x}\mathcal{F}\{\cos\omega_s t\}$$

which gives the result by taking $\varphi_x = \pi/2$ and recalling that $\cos(\omega_s t + \pi/2) = -\sin\omega_s t$.

ACKNOWLEDGMENT

The authors would like to dedicate this paper to the memory of Gregory C. Kozlowski whose talent and dedication was instrumental to the success of this work. In addition, we would like to express our gratitude to Drs. J. D. Michaelson, K. M. S. Hoo, and R. W. Phelps for their generous support and technical guidance throughout this effort.

REFERENCES

[1] *Amplitude and Phase Measurements of Frequency Translating Devices Using the HP 8510B Network Analyzer*, Product Note 8510-7, Hewlett-Packard Co., Sep. 1987.

[2] Thomas S. Laverghetta, *Modern Microwave Measurements and Techniques*. Norwood, MA.: Artech House, 1988.

[3] *HP 71500A Microwave Transition Analyzer Group Delay Personality*, Product Note 70820-10, Hewlett-Packard Co., Apr. 1994.

[4] C. J. Clark, A. A. Moulthrop, M. S. Muha, and C. P. Silva, "Transmission Response Measurements of Frequency Translating Devices," in *IEEE MTT-S Int. Microwave Symp. Dig.*, June 1996, pp. 1285–1288.

[5] *LabVIEW Virtual Instrumentation Software*, National Instruments Corp., Austin, TX.

[6] S. A. Maas, *Microwave Mixers*. Norwood, MA: Artech House, 1993, 2nd ed.

[7] M. Schwartz, W. R. Bennett, and S. Stein, *Communication Systems and Techniques*. New York: McGraw-Hill, 1966.

[8] A. Papoulis, *Signal Analysis*. New York: McGraw-Hill, 1977.

[9] M. C. Jeruchim, P. Balaban, and K. S. Shanmugan, *Simulation of Communication Systems*. New York: Plenum, 1992.

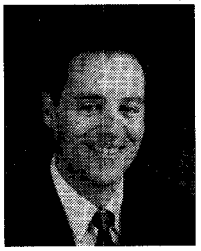

Christopher J. Clark was born in Washington, D.C., in 1960. He received the B.S.E.E. and M.S.E.E. degrees from the University of Maryland, College Park, in 1983 and 1986, respectively.

From 1984 to 1986, he worked for the Watkins–Johnson Company where he was responsible for the design and development of RF receiving systems. From 1986 to 1992, he worked for TRW Inc., where he developed microwave components for satellite applications. His primary focus was in the design of MESFET, HEMT, and HBT GaAs MMIC's for phased-array systems. He is currently an Engineering Specialist in the Electromagnetic Techniques Department, Communications Systems Subdivision, at The Aerospace Corporation, Los Angeles. His work involves the design of space communications systems and the development of hardware for digital satellite applications.

Mr. Clark is a member of Eta Kappa Nu and Tau Beta Pi.

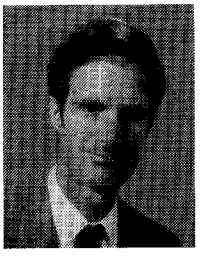

Andrew A. Moulthrop was born in San Francisco, CA, in 1955. He received the B.A. degree in physics in 1977 from the University of California, San Diego, and the Ph.D. degree in physics in 1984 from the University of California, Berkeley.

He is currently an Engineering Specialist in the Microwave/Millimeter-Wave Electronics Section in the Electromagnetic Techniques Department at The Aerospace Corporation, Los Angeles. His work involves the design, development and measurement of microwave components and systems. Previously, he worked as a Research Assistant at the University of California, Berkeley, where he co-developed a Josephson junction parametric amplifier, as well as measured various properties of superfluid helium.

Dr. Moulthrop is a member of Phi Beta Kappa.

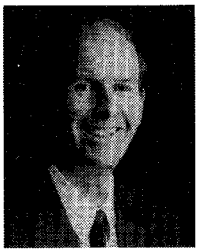

Michael S. Muha was born in Inglewood, CA, on February 21, 1958. He received the B.S. degree in physics in 1979 from the University of Southern California, Los Angeles, and the M.S. degree in applied physics in 1981 from the California Institute of Technology, Pasadena, where he worked on the design and development of millimeter-wave and far-infrared imaging antenna arrays.

He is currently manager of the Communication Techniques Section in the Electromagnetic Techniques Department at The Aerospace Corporation, Los Angeles, where he is working on the design, development and characterization of high data rate microwave communications systems.

Mr. Muha is a member of Phi Beta Kappa and Phi Kappa Phi.

Christopher P. Silva (S'81–M'89) was born on March 17, 1960, in Fortuna, CA. He received the B.S., M.S., and Ph.D. degrees, all in electrical engineering, in 1982, 1985, and 1993, respectively, from the University of California, Berkeley. His graduate work was supported mainly by a National Science Foundation Fellowship and a Lockheed Leadership Fellowship.

He is currently a Senior Member of the Technical Staff of the Electromagnetic Techniques Department, Communications Systems Subdivision, at The Aerospace Corporation, Los Angeles. He has been the principal investigator on several internally funded research projects addressing nonlinear microwave CAD, secure communications by means of chaos, and compensation of nonlinear satellite communications channels. In addition, he is currently heading a study on the nonlinear modeling and compensation of high data rate microwave communications systems in support of national advanced satellite programs. He is also involved with the application of wavelets analysis to CAD and communications signaling. Previously, he worked as a Postgraduate Researcher at the Electronics Research Laboratory, University of California, Berkeley, where he investigated the chaotic dynamics of nonlinear circuits and systems.

Dr. Silva is a member of Eta Kappa Nu, Tau Beta Pi, Phi Beta Kappa, the Society for Industrial and Applied Mathematics, and the American Mathematical Society.